NANO LETTERS

Letter

pubs.acs.org/NanoLett

Gibbs–Thomson Effect in Planar Nanowires: Orientation and Doping Modulated Growth

Youde Shen,[†] Renjie Chen,[‡] Xuechao Yu,[§] Qijie Wang,[§] Katherine L. Jungjohann,[∥] Shadi A. Dayeh,*[,‡] and Tom Wu*[,⊥]

[†]Division of Physics and Applied Physics, School of Physical and Mathematical Sciences, Nanyang Technological University, 637371 Singapore

[‡]Department of Electrical and Computer Engineering, University of California San Diego, La Jolla, California 92093, United States

[§]School of Electrical and Electronic Engineering, Nanyang Technological University, 50 Nanyang Avenue, 639798 Singapore

[∥]Center for Integrated Nanotechnologies, Sandia National Laboratories, Albuquerque, New Mexico 87185, United States

[⊥]Materials Science and Engineering, King Abdullah University of Science and Technology (KAUST), Thuwal 23955, Saudi Arabia

Supporting Information

ABSTRACT: Epitaxy-enabled bottom-up synthesis of self-assembled planar nanowires via the vapor–liquid–solid mechanism is an emerging and promising approach toward large-scale direct integration of nanowire-based devices without postgrowth alignment. Here, by examining large assemblies of indium tin oxide nanowires on yttria-stabilized zirconia substrate, we demonstrate for the first time that the growth dynamics of planar nanowires follows a modified version of the Gibbs–Thomson mechanism, which has been known for the past decades to govern the correlations between thermodynamic supersaturation, growth speed, and nanowire morphology. Furthermore, the substrate orientation strongly influences the growth characteristics of epitaxial planar nanowires as opposed to impact at only the initial nucleation stage in the growth of vertical nanowires. The rich nanowire morphology can be described by a surface-energy-dependent growth model within the Gibbs–Thomson framework, which is further modulated by the tin doping concentration. Our experiments also reveal that the cutoff nanowire diameter depends on the substrate orientation and decreases with increasing tin doping concentration. These results enable a deeper understanding and control over the growth of planar nanowires, and the insights will help advance the fabrication of self-assembled nanowire devices.

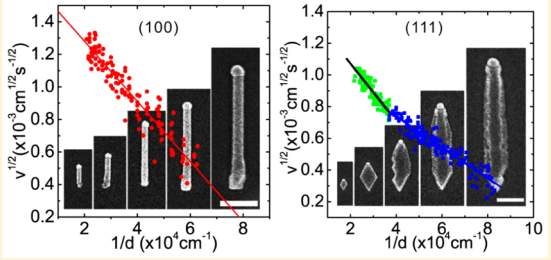

KEYWORDS: *nanowire, In_2O_3, ITO, Gibbs–Thomson effect, vapor–liquid–solid mechanism, surface energy*

Scaling of electronic and other devices into the nanoscale regime has fueled research on semiconductor nanowires (NWs), and such nanomaterials are emerging as promising building blocks for next-generation nanoscale devices and systems.[1,2] Although significant advances in the growth and applications of semiconductor NWs have been witnessed in the past decade,[3−7] it is still quite challenging to precisely align and integrate as-fabricated free-standing NWs into planar devices with high throughput. Most of the available approaches to assembling free-standing NWs into electronic devices suffer from issues like imperfect alignment, mechanical damage, and solution contamination.[8,9] In contrast, there have been innovative works on growing planar NWs in a single step from patterned growth seeds, which emerged as a novel and simple route toward integrating as-fabricated NWs into electronic devices without the need of additional postgrowth alignment steps.[10] Although there have been significant progresses in controlling the dimensions and growth directions of planar NWs,[11−15] deeper understanding of the growth mechanism and size scaling of planar NWs is urgently needed to further advance this field.

The thermodynamics of size-dependent NW growth is generally described by the well-known Gibbs–Thomson (G–T) effect, which claims a reduction of the supersaturation, the driving force for growth, when the size of NWs decreases.[16] G–T effect is ubiquitous in the nanomaterials synthesis except for systems with mass-transport-limited growth where surface collection of reactants dictates a reverse G–T effect (enhancement of growth rate at small sizes).[17−19] Givargizov was the first to experimentally reveal the G–T effect in the vapor–liquid–solid (VLS) growth of Si microwires about four decades ago and verified the quadric dependence of their growth velocity on supersaturation.[20] His observations proved applicable in recent NW studies via vapor-phase or solution-phase growth approaches.[21−29] As a major result of his model, NWs with larger diameters grow faster than the NWs with smaller diameters, and the growth of NWs will cease when the size of metal nanoparticles (NPs) is smaller than a certain cutoff

Received: March 10, 2016
Revised: May 24, 2016
Published: June 2, 2016

ACS Publications © 2016 American Chemical Society

DOI: 10.1021/acs.nanolett.6b01037
Nano Lett. 2016, 16, 4158–4165

diameter. Although the G−T effect is widely recognized for elucidating the growth of free-standing/vertical NWs, its applicability in the emerging planar NW growth is yet to be explored.

In this work, we demonstrate for the first time that the G−T effect governs the growth of planar NWs. As a model system, indium tin oxide (ITO) NWs were grown on yttria-stabilized zirconia (YSZ) substrates with tailored orientations. We focused our studies on ITO NWs due to their unique properties such as high transparency and conductivity, which enable their potential application as nanoscale transparent electrodes in LEDs, solar cells, displays, and thin-film transistors.[30−36] Recently, we reported the growth of planar ITO NWs with different exposed facets on oriented YSZ substrates.[37] In addition, the tin concentration in ITO NWs was modulated from 1% to 6% by changing the source composition, which gives additional means to tailor the free energies of NW surfaces.[38] These attributes position the ITO NW as a compelling platform to study the G−T effect in planar NW growth. Our results not only confirmed the validity of G−T effect in planar NWs but also revealed the impacts of doping and substrate surface orientation on the NW morphology and growth dynamics.

In order to systematically modulate the size of ITO NWs, we used electron-beam lithography (EBL) to pattern Au discs with diameters in the range of 60 to 870 nm and a fixed thickness of 20 nm (see Supporting Information Figure S1). The pitch between two adjacent discs was set to 10 μm in order to minimize synergetic effects between the NWs.[39] In the vapor transport growth, the growth temperature is 850 °C, and the growth time is 3−8 min. The source powder was composed of In_2O_3:SnO_2:C with a weight ratio of 0.6:0.4:1.

Figure 1 shows the representative scanning electron microscope (SEM) images of as-fabricated ITO NWs on [100]-, [110]-, and [111]-oriented YSZ substrates. The NWs grown on [100]-oriented YSZ substrates have a rectangular cross-section (Figure 1a) and are referred as (100)-R NWs. They showed four-fold symmetry (see Supporting Information Figure S2), and the length of the NWs increased with the diameter of the growth seed NPs, demonstrating a size-dependent growth velocity. On [110]-oriented YSZ substrates, two growth directions, [110] and [100], were observed with distinct NW morphologies (Figure 1b,c). The [110]-oriented NWs on (110) YSZ have a rectangular cross-section and are referred as (110)-R, whereas the [100]-oriented NWs on (110) YSZ have triangular cross-section and are referred as (110)-T. Different from the cases of growth on [100]- and [110]-oriented YSZ substrates, the ITO NWs grown on [111]-oriented YSZ substrate (Figure 1d) were characterized with a hexagonal cross-section composing of (113) sidewalls, and they also displayed a size-dependent growth behavior. Overall, there is a strong correlation between the NW length and their cross-sectional dimensions in all ITO NWs regardless of their morphology and orientation details.

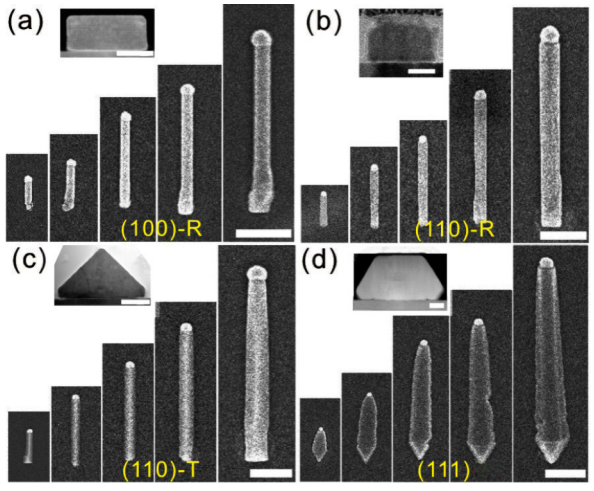

Figure 1. Evolution of dimension and morphology of ITO NWs grown on YSZ substrates. (a) SEM images of ITO NWs with different dimensions grown on a [100]-oriented YSZ substrate. (b,c) SEM images of [110]- and [100]-oriented ITO NWs grown on a [110]-oriented YSZ substrate, respectively. (d) SEM images of ITO NWs grown on a [111]-oriented YSZ substrate. The diameters of the Au growth seeds in (a−d) are 100, 200, 300, 400, and 500 nm, respectively. The insets in (a−d) show the corresponding cross-sectional TEM images of the ITO NWs. Scale bars are 1 μm for (a−d) and 20 nm for the insets.

In the applications of ITO NWs, tin doping was frequently used to tailor their optical and electronic properties,[38,40] and this composition tuning is associated with the modification of surface energies. To the best of our knowledge, the effect of doping on the growth habit of planar NWs has not been investigated so far. In our experiments, we intentionally modulated the tin doping level in the ITO NWs by reducing the SnO_2 weight ratio in the source powder and studied such a composition effect on the size-dependent growth behavior. We used three types of source powders with the In_2O_3:SnO_2:C weight ratios of 0.6:0.4:1, 0.8:0.2:1, and 0.9:0.1:1. The Supporting Information Figure S2 shows the corresponding SEM images of the as-grown NWs on YSZ substrates with different orientations. As shown in Figure 2a−f, the length (Figure 2a−c) and growth velocity (Figure 2d−f) of ITO NWs on [100]- and [110]-oriented YSZ substrates are clearly size-dependent, which gives us an additional parameter to tune the growth behavior of planar NWs.

The supersaturation in NWs, which is the driving force for NW growth, is size-dependent according to the G−T equation[41]

$$\Delta\mu = \Delta\mu_0 - \frac{4\Omega\alpha_{vs}}{d} \quad (1)$$

where $\Delta\mu_0$ denotes the supersaturation between vapor and solid with infinite radius of curvature, that is, planar limit, Ω the atomic volume of the growth species, d the diameter of the liquid-state growth seeds, and α_{vs} the average surface energy. Prior works reported that quadratic dependence of growth velocity on supersaturation emerges when the surface diffusion on NW surfaces is negligible,[42−48] a scenario adopted here for the ITO NW growth. Therefore, we assumed the average NW growth velocity ($v = l/t$) to depend quadratically on the supersaturation, that is, $v = b(\Delta\mu/kT)^2$, where b is a kinetic coefficient of crystallization, k the Boltzmann's constant, and T the temperature. Thus, eq 1 can be rearranged as

$$\sqrt{v} = \sqrt{b}\frac{\Delta\mu_0}{kT} - \sqrt{b}\frac{4\Omega\alpha_{vs}}{kT}\frac{1}{d} \quad (2)$$

According to this equation, the square root of growth velocity has a linear relationship with the reciprocal of growth seed NP diameter. If we set $v = 0$, we get the so-called cutoff diameter

DOI: 10.1021/acs.nanolett.6b01037
Nano Lett. 2016, 16, 4158−4165

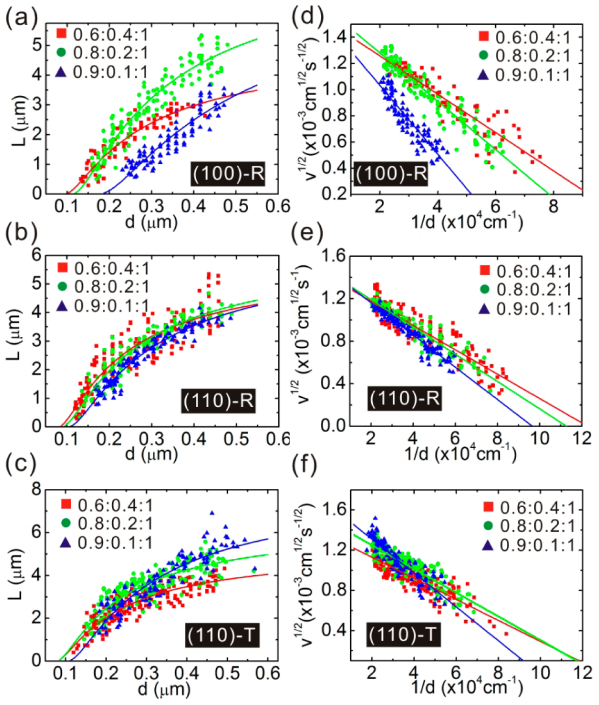

Figure 2. Length and growth velocity of ITO NWs on YSZ substrates with different orientations. Length of NWs grown on [100]-oriented substrate (panel a) and [110]-oriented substrate (panel b for type (110)-R NWs and panel c for type (110)-T NWs) as a function of growth seed NP diameter. Square root of the growth velocity as a function of reciprocal of the growth seed NP diameter for NWs grown on [100]-oriented substrate (panel d) and [110]-oriented substrate: panel e for (110)-R NWs and panel f for (110)-T NWs. In (a–f), the colored symbols indicate the different tin concentrations in sources, that is, the weight ratios of $In_2O_3/SnO_2/C$. The solid lines are fittings to the G–T equations.

$$d_c = \frac{4\Omega}{\Delta\mu_0}\alpha_{vs} \tag{3}$$

which is the diameter at which the NW growth ceases. Equations 1–3 are the general forms of the G–T equation formulated for vertical cylindrical NWs.[20] In our case, the oxide NWs grow laterally on YSZ substrates and their cross sections are not round. Therefore, appropriate adjustments to the surface energy terms of the G–T equation become necessary. As shown in the later discussions, the relationship between the NW growth velocity and the NP diameter remains essentially the same as those in eq 1–3. Furthermore, despite of the rich morphologies of such planar NWs, we assumed the diameters of the liquid-state growth seeds to be identical to those of the Au NPs observed in SEM images. Here, we note that potential in situ TEM experiments might provide better approximations of the thermodynamic terms.

In every growth run, the ITO NWs with different diameters and orientations grew simultaneously under the same growth conditions; therefore, the kinetic coefficient b, the atomic volume of the growth species Ω, and the bulk supersaturation $\Delta\mu_0$ are considered to be the same. However, the ITO NWs with different compositions exhibit different b and $\Delta\mu_0$, which leads to distinct cutoff diameters. As shown in Figure 2a–c, we fit the data of NW length against Au NP size according to eq 2 with a quadratic function. One immediate observation is that the cutoff diameter increases with decreasing tin doping concentration. Figure 2d–f present the linear fitting of the square root of growth velocity ($\sqrt{v}$) as a function of the reciprocal of Au NP size ($1/d$). Remarkably, the growth behaviors of (100)-R and (110)-R ITO NWs are in good agreement with the G–T effect despite of their different morphologies and tin doping levels. We note here that the fits of (110)-T NWs could be less accurate presumably due to the deviation of the triangular cross section of such NWs from that of round-shaped growth seeds. The individual cutoff diameters of ITO NWs were extracted from these fittings and listed in Table 1. These cutoff values are larger than those in our previous report,[37] highlighting the significant influence of growth conditions on the growth thermodynamics (see Supporting Information S3). The clear trend that the cutoff diameter decreases with increasing tin doping concentration can be attributed to the decrease of surface energy; particularly, it has been reported that ITO has a much lower surface energy than indium oxide,[49–53] and thus, the cutoff diameter will decrease with increasing tin doping level according to eq 3. Meanwhile, the cutoff diameters of ITO NWs also show a dependence on the substrate orientation, which will be discussed later in detail.

Table 1. Calculated Cutoff Diameters d_c[a] for ITO NWs Grown on YSZ Substrates with Varied Orientation and Tin Doping Concentration

source composition (In_2O_3:SnO_2:C)	(100)-R	(110)-R	(110)-T	(111)-W	(111)-R
0.6:0.4:1 (wt %)	94	81	78	92	57
0.8:0.2:1 (wt %)	112	89	80	127	87
0.9:0.1:1 (wt %)	169	104	102	135	71

[a]In nm.

In contrast to the growth behaviors of ITO NWs on [100]- and [110]-oriented substrates, ITO NWs grown on [111]-oriented YSZ substrate presented a more complex scenario. When the Au NPs are small, the ITO nanostructures displayed a rhombus shape, which is shown in the top SEM views in Figure 3a and 3b. In contrast, when the Au catalyst NPs are large, a NW-like shape was observed. As shown in Figure 3c, the atomic force microscopy (AFM) images show that the top surface of the NW is flat and the sidewalls of the NW are rough and multifaceted. We denote the rhombus-shaped NWs as (111)-R and the wire-shaped NWs as (111)-W.

In Figure 3d–f, the lengths of ITO NWs grown on (111) YSZ substrate with different tin doping levels are shown as a function of the NP diameter. Unlike the cases in Figure 2a–c, the data cannot be fitted by a single quadratic function, which means that the growth behaviors of (111)-R and (111)-W NWs are different. This trend is more obvious in the plot of $\sqrt{v}$ *vs* $1/d$, as shown in Figure 3g–i. Therefore, these data were separated into two regimes: rhombus-shaped growth regime and wire-shaped growth regime. Accordingly, the data in Figure 3d–i were fitted by two quadratic functions. From these fittings, the cutoff diameters were obtained and listed in Table 1. As expected, the cutoff diameter for (111)-W NWs increases with decreasing tin doping concentration, which is consistent with the cases of NWs on [100]- and [110]-oriented substrates. However, the cutoff diameter for (111)-R NWs does not follow this trend, which may be due to their imperfect rhombus shape. The transition point from wire-shaped growth to rhombus-shaped growth, that is, the intersection point of two fitting

DOI: 10.1021/acs.nanolett.6b01037
Nano Lett. 2016, 16, 4158–4165

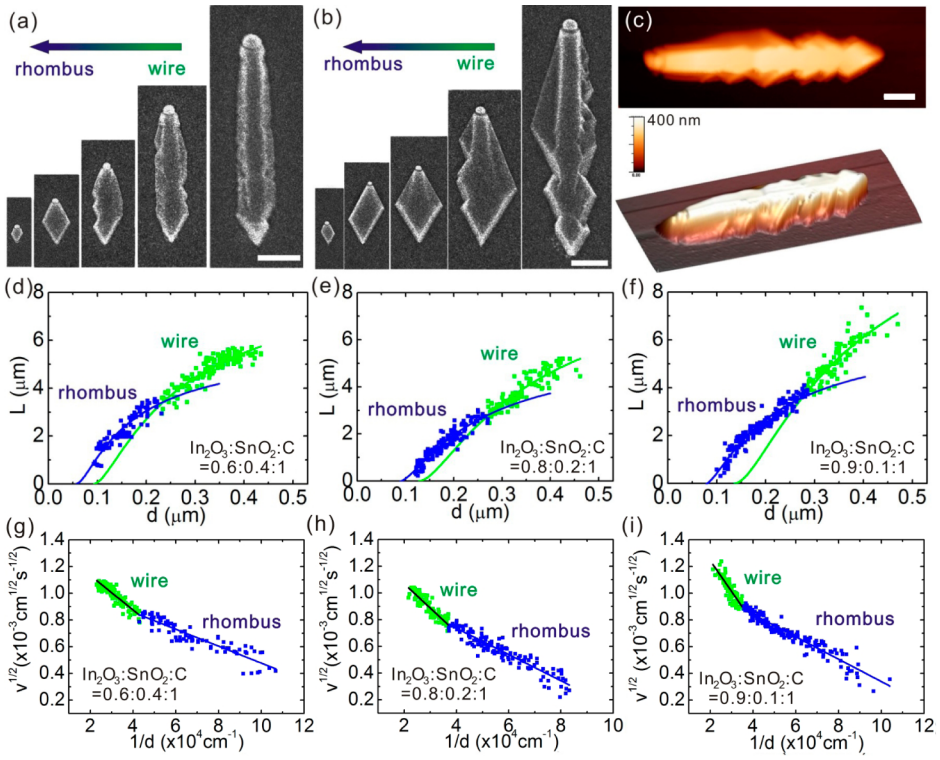

Figure 3. Morphology and growth velocity of ITO NWs on [111]-oriented YSZ substrates. (a,b) SEM images of NWs grown on a [111]-oriented YSZ substrate. The weight ratios of $In_2O_3/SnO_2/C$ in sources are 0.8:0.2:1 for (a) and 0.9:0.1:1 for (b). The morphology is NW-like when the growth seed NPs are large, while rhombus-like nanostructures were observed for smaller NPs. (c) AFM image of the NW in (b), showing faceted edges. (d–f) Length and (g–i) growth velocity of NWs grown on [111]-oriented YSZ substrates as a function of growth seed NP diameter with different tin concentrations in sources. The solid lines are fittings to the G–T equations. Scale bars are 1 μm in all images.

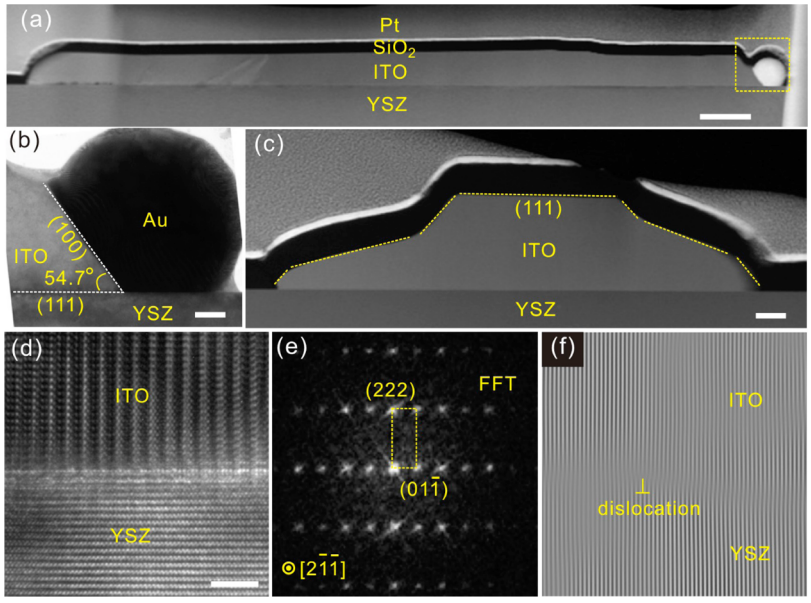

Figure 4. TEM characterization of ITO NWs grown on [111]-oriented YSZ substrate. (a) Cross-sectional HAADF TEM image of the lateral NW. Scale bar is 1 μm. (b) Zoom-in bright field (BF) TEM image of the trijunction of growth seed NP, NW, and substrate. The interface between NW and growth seed NP forming an angle of 54.7° with respect to YSZ substrate surface is ITO (100) plane. Scale bar is 50 nm. (c) TEM image of axial cross-section of NW. The sidewall is composed of several high-index facets. Scale bar is 100 nm. (d) High-resolution TEM (HR-TEM) image of the interface between ITO NW and YSZ substrate. Scale bar is 2 nm. (e) Fast Fourier transform (FFT) pattern of the axial cross-section of NW. (f) Inversed FFT from ITO [211] and YSZ [211], where the edge dislocation at the ITO/YSZ interface is denoted.

curves, shifts from 230 to 277 nm with decreasing tin doping level, which indicates that the tin doping promotes the growth of regular shaped NWs.

In order to better understand the morphology of ITO NWs grown on [111]-oriented YSZ substrates (Figure 3b), we performed high-angle annular dark-field (HAADF) TEM and

DOI: 10.1021/acs.nanolett.6b01037
Nano Lett. 2016, 16, 4158–4165

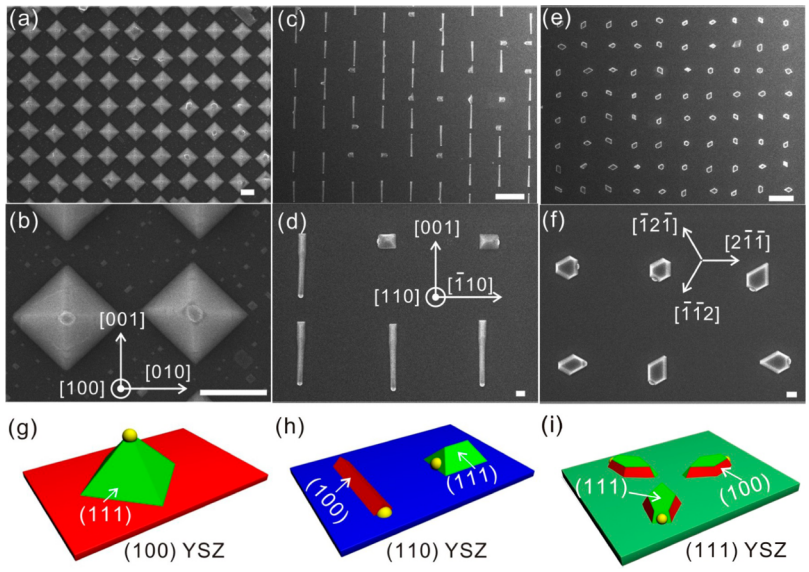

Figure 5. Morphology of IO nanostructures grown on YSZ substrates with different orientations. (a,b), (c,d), and (e,f) are SEM images of IO nanostructures grown on [100]-, [110]-, and [111]-oriented substrates at different magnifications, respectively. Scale bars are 1 μm in (a,b), (d), (f) and 5 μm in (c) and (e). (g–i) Corresponding schematics illustrating the morphology of IO nanostructures grown on [100]-, [110]-, and [111]-oriented YSZ substrates, respectively. The plane indexes of exposed surfaces are denoted.

energy dispersive X-ray (EDX) mapping experiments. The lateral and axial cross-sectional samples were prepared by applying focused ion beam (FIB) milling and in situ lift-out (INLO) techniques (see Supporting Information Figure S4). As shown in the lateral cross-section HAADF TEM image (Figure 4a), the thickness of the NW is quite uniform, which is consistent with the AFM result (Figure 3c). In the zoom-in TEM image of the trijunction of growth seed, NW and substrate (Figure 4b), the NW/NP interface forming an inclined angle of approximately 54.7° with respect to the substrate surface was identified as the ITO (100) plane based on the crystallographic relationship, which is consistent with our previous observations.[36,37] The axial cross-sectional image in Figure 4c shows that the NW sidewalls are composed of high-index facets. The TEM image (Figure 4d) and the corresponding fast Fourier transform (FFT) patterns (Figure 4e) taken near the NW/substrate interface confirm the expected good epitaxial relationship between the ITO NW and the YSZ substrate. As shown in Figure 4f, some misfit edge dislocations were observed at the interface. Finally, the EDX mappings of axial and lateral cross sections (Supporting Information Figure S5) show that the tin dopants are distributed uniformly in the ITO NWs.

The rough and multifaceted morphology of ITO NWs grown on ⟨111⟩-oriented YSZ substrate as shown in Figure 3a,b might arise from the competition between top and sidewall surface energies. It is clear that the surface energy of ITO increases with decreasing tin doping concentration such that the NW sidewalls become unstable and multifaceted. Furthermore, the (111) planes have the lowest surface energy and the nanostructures are prone to form (111) faceted planes, resulting in the dominant rhombus-shaped nanostructures in the initial growth stage. Finally, the faceting behavior of such oxide nanostructures seems to imply an underlying relationship with the Plateau–Rayleigh growth instability as reported recently for the synthesis of diameter-modulated core–shell NWs.[54] We believe that harnessing the kinetic facet growth and the crystal plane energetics might enable the realization of planar nanostructures with designed morphological complexities.

The observation of tin doping effects on the growth of planar ITO NWs motivated us to further study the undoped indium oxide (IO) NWs. As shown in Figure 5, the undoped IO nanostructures exhibit quite different growth behaviors on YSZ substrates with different orientations. Pyramid islands are formed on [100]-oriented YSZ substrate (Figure 5a,b) and the simple morphology of the IO nanostructures obtained here are consistent with the report from Egdell and co-workers.[53,55,56] As illustrated in Figure 5g, the exposed surfaces of the pyramids are (111) planes, which is consistent with the lowest surface energy of (111) planes in IO.[53]

As shown in Figure 5c,d, the morphology of IO NWs grown on [110]-oriented YSZ substrate is more complex than the case on [100] substrate. One prominent feature is that the [100]-oriented IO NWs are much longer than the [110]-oriented ones. The [110]-oriented IO NWs are so short that they are almost pyramid-shaped. Similar [110]-oriented pyramid-shaped IO NWs were also reported by Zhang et al. for molecular beam epitaxy growth without the usage of any seed.[53] However, different from their results, we obtained additional [100]-oriented NWs, indicating the strong dependence of the NW morphology on the growth method. In the VLS growth process, the nucleation energy is significantly reduced at the interfaces between the liquid growth seeds and the solid NWs, whereas in the molecular beam epitaxy growth process,[53] without the growth seeds, the energetic differences between low-index surfaces of IO clearly favors the growth of [110]-oriented NWs.

In Figure 5e,f, the IO nanostructures grown on the [111]-oriented YSZ substrate appear to be rhombus-shaped islands. These rhombus-shaped islands point to the three equivalent [112] directions with a 3-fold symmetry which conforms to the epitaxial relationship between IO and YSZ. Such IO nanostructures have not been reported in literature, but the minimization of total surface energy clearly plays an important role on the growth morphology. It is interesting to compare

DOI: 10.1021/acs.nanolett.6b01037
Nano Lett. 2016, 16, 4158–4165

with the case of growing ITO NWs on [111]-oriented YSZ substrate shown in Figure 1d and Figure 4. In the ITO case, (113) and other high-index facets were observed. However, in the IO case, NWs with such high-index surfaces could not grow, and only rhombus-shaped IO nanostructures with (111) and (100) facets were formed (Figure 5i). This strong contrast indicates that compared with IO, ITO has much lower surface energies, which is consistent with the known lowering of surface energies of such oxides with doping.

Regarding the growth dynamics, the G−T eq 1 developed for the case of vertical cylindrical NWs must be modified for the planar NWs investigated in the present work. Such planar NWs are featured with faceted surfaces, and both the surface energies of exposed NW facets and the NW/substrate interface energies should be considered.[57] Our TEM and SEM observations provided essential information on NW geometries. As shown in Figure 6, both the (100)-R NWs and the (110)-R NWs have a

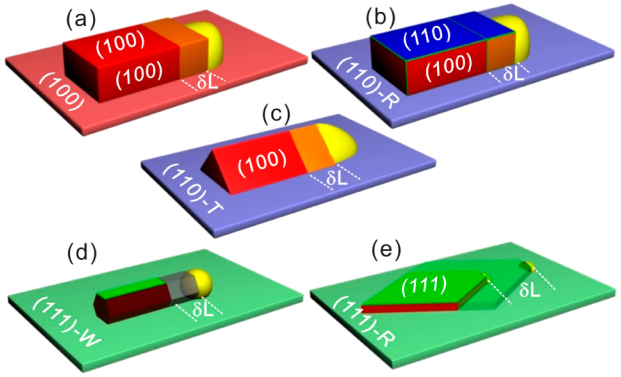

Figure 6. Schematic illustration of the ITO NWs on YSZ substrates with different growth orientations and exposed surfaces. (a) Planar ITO NWs on (100) YSZ substrate. (b) [110]-oriented NWs with rectangular cross-section on (110) YSZ substrate. (c) [100]-oriented NWs with triangle cross section on (110) YSZ substrate. (d) Wire-shaped nanostructures on (111) YSZ substrate. (e) Rhombus-shaped nanostructures on (111) YSZ substrate.

rectangular cross-section with a width-to-height ratio of approximately 2:1; (110)-T NWs have a triangular cross-section; (111)-W NWs have a hexagonal cross-section and (111)-R NWs have a rhombus shape. In the following, we will derive the extended G−T equation by considering the Gibbs free energies involved in the growth of ITO NWs. The general methodology should be applicable to the growth of planar NWs with other compositions and morphologies.

Under fixed growth conditions, the Gibbs free energy change (ΔG) during the NW growth can be expressed as

$$\Delta G = \Delta N(-\Delta\mu_0) + \Delta S_{vs}\alpha_{vs} + \Delta S_{inter}\alpha_{inter} - \Delta S_{inter}\alpha_{ysz} \quad (4)$$

where ΔN denotes the increased number of atoms of the growth species, $\Delta\mu_0$ the supersaturation with infinite radius of curvature, ΔS_{vs} the surface area increase, α_{vs} the surface energy, ΔS_{inter} the interface area increase, α_{inter} the interface energy, and α_{ysz} the surface energy of substrate (YSZ). Hence, the supersaturation in planar NWs is given by

$$\Delta\mu = -\frac{\Delta G}{\Delta N} = \Delta\mu_0 - \frac{\Delta S_{vs}\alpha_{vs} + \Delta S_{inter}\alpha_{inter} - \Delta S_{inter}\alpha_{ysz}}{\Delta N} \quad (5)$$

On the basis of the geometries of planar NWs shown in Figure 6, the corresponding G−T equations can be derived as

$$\Delta\mu = \Delta\mu_0 - \frac{\Omega}{d}(4\alpha_{vs,(100)} + 2\alpha_{inter,(100)} - 2\alpha_{ysz,(100)}) \quad (6a)$$

$$\Delta\mu = \Delta\mu_0 - \frac{\Omega}{d}(2\alpha_{vs,(100)} + 2\alpha_{vs,(110)} + 2\alpha_{inter,(110)} - 2\alpha_{ysz,(110)}) \quad (6b)$$

$$\Delta\mu = \Delta\mu_0 - \frac{\Omega}{d}(4\sqrt{2}\,\alpha_{vs,(100)} + 4\alpha_{inter,(110)} - 4\alpha_{ysz,(110)}) \quad (6c)$$

$$\Delta\mu = \Delta\mu_0 - \frac{\Omega}{d}\left(\frac{16}{3\sqrt{3}}\alpha_{vs,(113)} + \frac{4}{3\sqrt{3}}\alpha_{vs,(111)} + \frac{4}{3\sqrt{3}}\alpha_{inter,(111)} - \frac{4}{3\sqrt{3}}\alpha_{ysz,(111)}\right) \quad (6d)$$

$$\Delta\mu = \Delta\mu_0 - \frac{\Omega}{d}(2\alpha_{vs,(111)} + 2\alpha_{inter,(111)} - 2\alpha_{ysz,(111)}) \quad (6e)$$

where Ω is the atomic volume and d the growth seed NP diameter. The derivation details for eq 6a−6e are given in Supporting Information. Because the G−T eqs 6a−6e have the similar structures, they can be rewritten as

$$\Delta\mu = \Delta\mu_0 - \frac{\Omega}{d}\alpha_{eff} \quad (6)$$

with α_{eff} being the effective surface energy. When $\Delta\mu = 0$, we get the cutoff diameter for planar NWs

$$d_{c,p} = \frac{\Omega}{\Delta\mu_0}\alpha_{eff} \quad (7)$$

On the one hand, eqs 6 and 7 have the similar form as that of eqs 1 and 3, thus the analysis based on the general G−T equations and the fitting shown in Figures 2 and 3 remain valid. On the other hand, the G−T equations for planar NWs depend on the morphology details of faceted NWs and their interfaces with substrates. Therefore, the morphology and the cutoff diameter of the planar NWs provide valuable insights on the surface and interface energies of the grown materials.

The fact that planar ITO NWs were observed instead of the vertical ones indicates that ITO/YSZ interface energy is quite small, which is consistent with the good lattice match of ~1.6% between ITO and YSZ.[58,59] As a general principle of crystal growth, the exposed surfaces are associated with high energies because of the dangling chemical bonds, and thus the total exposed surface area should be minimized. In fact, by comparing the growth behaviors of planar NW, we can derive valuable information on the surface energies. Let us use the ITO NWs grown on [100]- and [110]-oriented YSZ substrates as an example. Here, we ignore the interface energies because of the small lattice mismatch between ITO and YSZ and their identical cubic structure; the misfit dislocations shown in Figure 4f further help release the interfacial stress. As shown in Figure

DOI: 10.1021/acs.nanolett.6b01037
Nano Lett. 2016, 16, 4158−4165

6a,b, the sidewalls of (100)-R and (110)-R NWs are both (100) facets and the sidewall dimensions are similar. Thus, their effective surface energies in eqs 6a and 6b are determined by the top facets, that is, (100) plane for (100)-R and (110) plane for (110)-R. The order of surface energy for (100) and (110) planes is still under debate: Zhang et al. reported that the surface energy of the (100) facets of undoped In_2O_3 is larger than that of the (110) facets, using first-principle calculations;[53] in contrast, Hao et al. suggested the opposite based on their experimental observations.[60] In the present work, as shown in Table 1, the (100)-R NWs have a larger cutoff diameter than the (110)-R NWs, indicating that the (100)-R NWs has a higher effective surface energy than that of (110)-R NWs and the (100) plane has a higher surface energy than the (110) plane.

For the NWs grown on [111]-oriented YSZ substrates, (111)-W NWs have five exposed facets (one (111) facet and four (113) facets), and the four (113) facets are high-index planes. Meanwhile, (111)-R NWs have three exposed facets and the large top facet is the low-energy (111) plane. Therefore, the (111)-W NWs have a higher effective surface energy and a bigger cutoff diameter than the (111)-R ones, which is consistent with experimental observations (Table 1). Interestingly, the majority facets of the (111)-R structures are low-energy (111) surfaces, which results in the smallest cutoff diameter. Overall, the observation of G−T effect and the variation of cutoff diameters in planar NWs provide valuable information on the surface energies of oxide nanostructures.

In summary, we investigated the existence of G−T effect in the growth of planar NWs for the first time using planar ITO NWs with different tin doping concentrations grown on [100]-, [110]-, and [111]-oriented YSZ substrates as a prototypical example. Our results showed conclusively that the G−T effect could be modulated by both substrate orientation and NW composition, leading to rich NW morphology and growth behavior. In particular, the cutoff diameter of ITO NWs increases with decreasing tin doping concentration, and the lowest cutoff diameter was obtained for (111)-R NWs. By modeling the G−T effect, we elucidated the thermodynamic implications on the structural characteristics of planar ITO NWs, and we further propose that one can better design planar nanostructures with the knowledge of surface energies associated with different crystal planes. This in-depth understanding of the G−T effect in the planar NW growth will enable the controlled synthesis of planar NWs with desired geometries and properties, facilitating their large-scale integration into functional devices.

■ ASSOCIATED CONTENT

Supporting Information

The Supporting Information is available free of charge on the ACS Publications website at DOI: 10.1021/acs.nanolett.6b01037.

The methods, SEM images, the FIB process, and EDX results. (PDF)

■ AUTHOR INFORMATION

Corresponding Authors

*E-mail: sdayeh@ece.ucsd.edu.

*E-mail: Tao.Wu@kaust.edu.sa.

Notes

The authors declare no competing financial interest.

■ ACKNOWLEDGMENTS

The FIB preparations, AFM and TEM characterizations in this work were performed at the Center for Integrated Nanotechnologies (CINT), a U.S. Department of Energy, Office of Basic Energy Sciences User Facility at Los Alamos National Laboratory (Contract DE-AC52-06NA25396) and Sandia National Laboratories (Contract DE-AC04-94AL85000). S.A.D. acknowledges support of an NSF CAREER Award under ECCS-1351980 and an NSF DMR-1503595 award.

■ REFERENCES

(1) Thelander, C.; Agarwal, P.; Brongersma, S.; Eymery, J.; Feiner, L. F.; Forchel, A.; Scheffler, M.; Riess, W.; Ohlsson, B. J.; Gösele, U.; Samuelson, L. *Mater. Today* **2006**, *9* (10), 28−35.

(2) Lieber, C. M.; Wang, Z. L. *MRS Bull.* **2007**, *32* (2), 99−108.

(3) Xia, Y. N.; Yang, P. D.; Sun, Y. G.; Wu, Y. Y.; Mayers, B.; Gates, B.; Yin, Y. D.; Kim, F.; Yan, Y. Q. *Adv. Mater.* **2003**, *15* (5), 353−389.

(4) Algra, R. E.; Verheijen, M. A.; Borgström, M. T.; Feiner, L. F.; Immink, G.; van Enckevort, W. J. P.; Vlieg, E.; Bakkers, E. *Nature* **2008**, *456* (7220), 369−372.

(5) Bierman, M. J.; Jin, S. *Energy Environ. Sci.* **2009**, *2* (10), 1050−1059.

(6) Qu, Y.; Duan, X. *Chem. Soc. Rev.* **2013**, *42* (7), 2568−2580.

(7) Dasgupta, N. P.; Sun, J. W.; Liu, C.; Brittman, S.; Andrews, S. C.; Lim, J.; Gao, H. W.; Yan, R. X.; Yang, P. D. *Adv. Mater.* **2014**, *26* (14), 2137−2184.

(8) Wang, M. C. P.; Gates, B. D. *Mater. Today* **2009**, *12* (5), 34−43.

(9) Long, Y. Z.; Yu, M.; Sun, B.; Gu, C. Z.; Fan, Z. Y. *Chem. Soc. Rev.* **2012**, *41* (12), 4560−4580.

(10) Nikoobakht, B.; Wang, X. D.; Herzing, A.; Shi, J. *Chem. Soc. Rev.* **2013**, *42* (1), 342−365.

(11) Fortuna, S. A.; Wen, J. G.; Chun, I. S.; Li, X. L. *Nano Lett.* **2008**, *8* (12), 4421−4427.

(12) Nikoobakht, B.; Herzing, A. *ACS Nano* **2010**, *4* (10), 5877−5886.

(13) Yoo, Y.; Yoon, I.; Lee, H.; Ahn, J.; Ahn, J. P.; Kim, B. *ACS Nano* **2010**, *4* (5), 2919−2927.

(14) Tsivion, D.; Schvartzman, M.; Popovitz-Biro, R.; von Huth, P.; Joselevich, E. *Science* **2011**, *333* (6045), 1003−1007.

(15) Schvartzman, M.; Tsivion, D.; Mahalu, D.; Raslin, O.; Joselevich, E. *Proc. Natl. Acad. Sci. U. S. A.* **2013**, *110* (38), 15195−15200.

(16) Dayeh, S. A.; Picraux, S. T. *Nano Lett.* **2010**, *10* (10), 4032−4039.

(17) Dubrovskii, V. G.; Cirlin, G. E.; Soshnikov, I. P.; Tonkikh, A. A.; Sibirev, N. V.; Samsonenko, Y. B.; Ustinov, V. M. *Phys. Rev. B: Condens. Matter Mater. Phys.* **2005**, *71* (20), 205325.

(18) Schmidt, V.; Senz, S.; Gösele, U. *Phys. Rev. B: Condens. Matter Mater. Phys.* **2007**, *75* (4), 045335.

(19) Dayeh, S. A.; Yu, E. T.; Wang, D. *Nano Lett.* **2009**, *9* (5), 1967−1972.

(20) Givargizov, E. I. *J. Cryst. Growth* **1975**, *31* (DEC), 20−30.

(21) Park, H. D.; Gaillot, A. C.; Prokes, S. M.; Cammarata, R. C. *J. Cryst. Growth* **2006**, *296* (2), 159−164.

(22) Zhang, X.; Lew, K.-K.; Nimmatoori, P.; Redwing, J. M.; Dickey, E. C. *Nano Lett.* **2007**, *7* (10), 3241−3245.

(23) Fröberg, L. E.; Seifert, W.; Johansson, J. *Phys. Rev. B: Condens. Matter Mater. Phys.* **2007**, *76* (15), 153401.

(24) Clark, T. E.; Nimmatoori, P.; Lew, K. K.; Pan, L.; Redwing, J. M.; Dickey, E. C. *Nano Lett.* **2008**, *8* (4), 1246−1252.

(25) Biswas, S.; O'Regan, C.; Petkov, N.; Morris, M. A.; Holmes, J. D. *Nano Lett.* **2013**, *13* (9), 4044−4052.

(26) Pinion, C. W.; Nenon, D. P.; Christesen, J. D.; Cahoon, J. F. *ACS Nano* **2014**, *8* (6), 6081−6088.

(27) Zhang, C.; Miao, X.; Mohseni, P. K.; Choi, W.; Li, X. *Nano Lett.* **2014**, *14* (12), 6836−6841.

(28) Biswas, S.; O'Regan, C.; Morris, M. A.; Holmes, J. D. *Small* **2015**, *11* (1), 103−111.

DOI: 10.1021/acs.nanolett.6b01037
Nano Lett. 2016, 16, 4158−4165

(29) Lee, J. M.; No, Y.-S.; Kim, S.; Park, H.-G.; Park, W. I. *Nat. Commun.* **2015**, *6*, 6325.
(30) Ju, S. Y.; Facchetti, A.; Xuan, Y.; Liu, J.; Ishikawa, F.; Ye, P. D.; Zhou, C. W.; Marks, T. J.; Janes, D. B. *Nat. Nanotechnol.* **2007**, *2* (6), 378−384.
(31) O'Dwyer, C.; Szachowicz, M.; Visimberga, G.; Lavayen, V.; Newcomb, S. B.; Torres, C. M. S. *Nat. Nanotechnol.* **2009**, *4* (4), 239−244.
(32) Li, S. Q.; Guo, P. J.; Zhang, L. X.; Zhou, W.; Odom, T. W.; Seideman, T.; Ketterson, J. B.; Chang, R. P. H. *ACS Nano* **2011**, *5* (11), 9161−9170.
(33) Yu, H. K.; Dong, W. J.; Jung, G. H.; Lee, J. L. *ACS Nano* **2011**, *5* (10), 8026−8032.
(34) Wu, H.; Hu, L. B.; Carney, T.; Ruan, Z. C.; Kong, D. S.; Yu, Z. F.; Yao, Y.; Cha, J. J.; Zhu, J.; Fan, S. H.; et al. *J. Am. Chem. Soc.* **2011**, *133* (1), 27−29.
(35) Dattoli, E. N.; Lu, W. *MRS Bull.* **2011**, *36* (10), 782−788.
(36) Gao, J.; Lebedev, O. I.; Turner, S.; Li, Y. F.; Lu, Y. H.; Feng, Y. P.; Boullay, P.; Prellier, W.; van Tendeloo, G.; Wu, T. *Nano Lett.* **2012**, *12* (1), 275−280.
(37) Shen, Y. D.; Turner, S.; Yang, P.; Van Tendeloo, G.; Lebedev, O. I.; Wu, T. *Nano Lett.* **2014**, *14* (8), 4342−4351.
(38) Gao, J.; Chen, R.; Li, D. H.; Jiang, L.; Ye, J. C.; Ma, X. C.; Chen, X. D.; Xiong, Q. H.; Sun, H. D.; Wu, T. *Nanotechnology* **2011**, *22* (19), 195706.
(39) Borgstrom, M. T.; Immink, G.; Ketelaars, B.; Algra, R.; Bakkers, E. *Nat. Nanotechnol.* **2007**, *2* (9), 541−544.
(40) Park, K. S.; Choi, Y. J.; Kang, J. G.; Sung, Y. M.; Park, J. G. *Nanotechnology* **2011**, *22* (28), 285712.
(41) Givargizov, E. I. *Highly Anisotropic Crystals*; Springer: New York, 1987; pp 100−112.
(42) Schubert, L.; Werner, P.; Zakharov, N. D.; Gerth, G.; Kolb, F. M.; Long, L.; Gösele, U.; Tan, T. Y. *Appl. Phys. Lett.* **2004**, *84* (24), 4968−4970.
(43) Johansson, J.; Svensson, C. P. T.; Mårtensson, T.; Samuelson, L.; Seifert, W. *J. Phys. Chem. B* **2005**, *109* (28), 13567−13571.
(44) Kodambaka, S.; Tersoff, J.; Reuter, M. C.; Ross, F. M. *Phys. Rev. Lett.* **2006**, *96* (9), 096105.
(45) Dubrovskii, V. G.; Sibirev, N. V. *J. Cryst. Growth* **2007**, *304* (2), 504−513.
(46) Dubrovskii, V. G.; Sibirev, N. V.; Cirlin, G. E.; Soshnikov, I. P.; Chen, W. H.; Larde, R.; Cadel, E.; Pareige, P.; Xu, T.; Grandidier, B.; et al. *Phys. Rev. B: Condens. Matter Mater. Phys.* **2009**, *79* (20), 205316.
(47) Mohammad, S. N. *J. Vac. Sci. Technol. B* **2010**, *28* (2), 329−352.
(48) Shakthivel, D.; Raghavan, S. *J. Appl. Phys.* **2012**, *112* (2), 024317.
(49) Kim, J. S.; Friend, R. H.; Cacialli, F. *J. Appl. Phys.* **1999**, *86* (5), 2774−2778.
(50) Paniagua, S. A.; Hotchkiss, P. J.; Jones, S. C.; Marder, S. R.; Mudalige, A.; Marrikar, F. S.; Pemberton, J. E.; Armstrong, N. R. *J. Phys. Chem. C* **2008**, *112* (21), 7809−7817.
(51) Hotchkiss, P. J.; Li, H.; Paramonov, P. B.; Paniagua, S. A.; Jones, S. C.; Armstrong, N. R.; Bredas, J. L.; Marder, S. R. *Adv. Mater.* **2009**, *21* (44), 4496−4501.
(52) Walsh, A.; Catlow, C. R. A. *J. Mater. Chem.* **2010**, *20* (46), 10438−10444.
(53) Zhang, K. H. L.; Walsh, A.; Catlow, C. R. A.; Lazarov, V. K.; Egdell, R. G. *Nano Lett.* **2010**, *10* (9), 3740−3746.
(54) Day, R. W.; Mankin, M. N.; Gao, R.; No, Y.-S.; Kim, S.-K.; Bell, D. C.; Park, H.-G.; Lieber, C. M. *Nat. Nanotechnol.* **2015**, *10* (4), 345−352.
(55) Bourlange, A.; Payne, D. J.; Jacobs, R. M. J.; Egdell, R. G.; Foord, J. S.; Schertel, A.; Dobson, P. J.; Hutchison, J. L. *Chem. Mater.* **2008**, *20* (14), 4551−4553.
(56) Zhang, K. H. L.; Bourlange, A.; Egdell, R. G.; Collins, S. P.; Bean, R. J.; Robinson, I. K.; Cowley, R. A. *ACS Nano* **2012**, *6* (8), 6717−6729.
(57) Zi, Y. L.; Jung, K.; Zakharov, D.; Yang, C. *Nano Lett.* **2013**, *13* (6), 2786−2791.
(58) Wan, Q.; Wei, M.; Zhi, D.; MacManus-Driscoll, J. L.; Blamire, M. G. *Adv. Mater.* **2006**, *18* (2), 234−238.
(59) Wan, Q.; Dattoli, E. N.; Fung, W. Y.; Guo, W.; Chen, Y. B.; Pan, X. Q.; Lu, W. *Nano Lett.* **2006**, *6* (12), 2909−2915.
(60) Hao, Y. F.; Meng, G. W.; Ye, C. H.; Zhang, L. D. *Cryst. Growth Des.* **2005**, *5* (4), 1617−1621.

DOI: 10.1021/acs.nanolett.6b01037
Nano Lett. 2016, 16, 4158−4165

Supporting Information

Gibbs-Thomson Effect in Planar Nanowires: Orientation and Doping Modulated Growth

Youde Shen,[†] Renjie Chen,[‡] Xuechao Yu,[▽] Qijie Wang,[▽] K. L. Jungjohann,[❖] Shadi A. Dayeh,[*, ‡] Tom Wu[*, §]

[†]Division of Physics and Applied Physics, School of Physical and Mathematical Sciences, Nanyang Technological University, 637371, Singapore,

[‡]Department of Electrical and Computer Engineering, University of California San Diego, La Jolla, California 92093, USA,

[▽]School of Electrical and Electronic Engineering, Nanyang Technological University, 50 Nanyang Ave., 639798, Singapore,

[❖]Center for Integrated Nanotechnologies, Sandia National Laboratories, Albuquerque, NM 87185, USA,

[§]Materials Science and Engineering, King Abdullah University of Science and Technology (KAUST), Thuwal 23955, Saudi Arabia.

*Correspondence and requests for materials should be addressed to S. A. Dayeh (sdayeh@ece.ucsd.edu) or T. Wu (Tao.Wu@KAUST.EDU.SA).

METHODS

Growth of ITO and IO nanostructures: ITO/IO NWs were grown on YSZ substrates with different orientations using the vapor transfer method in a horizontal furnace with controlled gas delivery and pumping. A mixture of In_2O_3, SnO_2 and graphite powder with weight ratios of 0.6:0.4:1, 0.8:0.2:0.1, 0.9:0.1:1 and 1:0:1 were used as the sources and placed at the center of the furnace quartz tube. YSZ substrates with patterned Au disc arrays (thickness: 20 nm) were placed about 9 cm downstream from the source. Argon gas with a fixed gas flow of 100 sccm (standard cubic centimeters per minute) was introduced as the carrier gas to transfer vapor from the source to the substrates. The pressure inside the tube was fixed at 30 mbar during NW growth. The heating rate of the furnace was fixed at 50 °C/min and the temperature overshoot was smaller than 5 °C. The growth temperature was kept at 850 ºC and the growth time was varied from 3 min to 8 min. After growth, in order to stop the growth as quickly as possible, the Ar gas was shut down immediately and the quartz tube was removed from the furnace and cooled down by fans.

Fabrication of patterned Au disc arrays: 4% 950K PMMA in Anisole (950 A4, MicroChem, Inc.) was first spin-coated on YSZ substrates (4000 rpm, 45 s) to achieve a thickness of ~180 nm. After electron beam writing using a Raith E-line system, the substrate was developed in a MIBK:IPA (1:3) solution for 30 s and washed in IPA solvent for 30 s. Ti (2 nm)/Au (20 nm) bilayers were deposited using electron beam evaporation, followed by a standard lift-off process in acetone.

Characterizations: The morphology of as-fabricated ITO/IO nanostructures was examined using field emission scanning electron microscopy (FESEM, JEOL JSM-6700F). The surface topographical measurements were performed with an atomic force microscope (AFM, DI Veeco). Cross-sectional samples for TEM investigation were prepared using a focused ion beam (FBI, FEI Nova 600) and Ar ion post cleaning (Fischione Model 1010 ion mill). TEM, STEM, and EDX elemental mapping were carried out on a FEI Tecnai F30 transmission electron microscope.

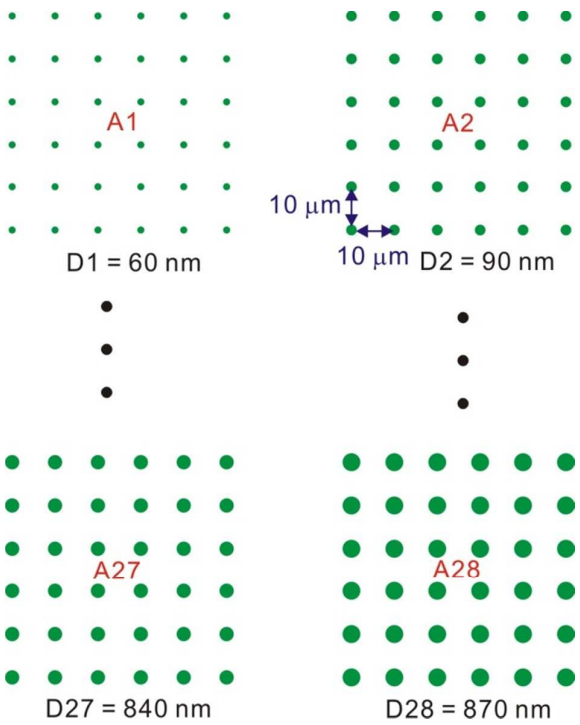

Figure S1. Schematic illustrating the patterned Au catalyst disc arrays. The diameters of disc arrays from A1 to A28 are increasing from 60 nm to 870 nm with a step of 30 nm. The pitch between two adjacent discs is 10 μm. In every catalyst disc array, there are 20×20 Au discs.

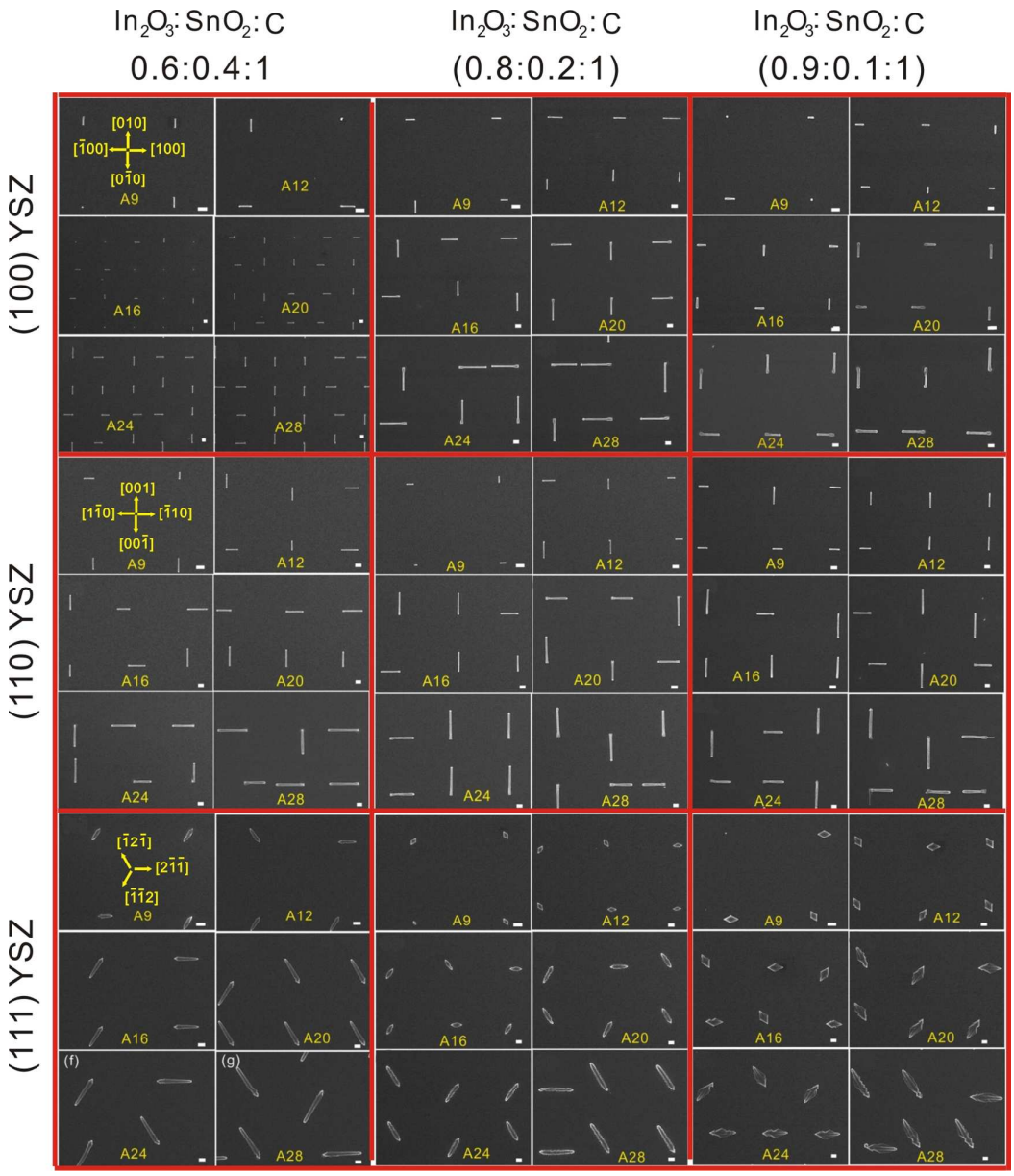

Figure S2. Morphology of ITO NWs with varied tin doping levels grown on oriented YSZ substrates. The source compositions (wt%) are In_2O_3:SnO_2:C=0.6:0.4:1, 0.8:0.2:1 and 0.9:0.1:1 and the YSZ substrate orientations are (111), (110), and (100). Scale bars are 1 μm.

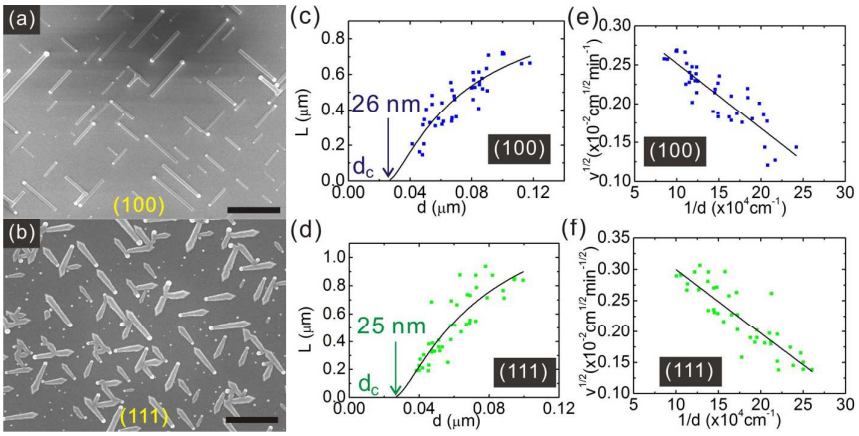

Figure S3. (a,b) SEM images of ITO NWs grown on [100]- and [111]-oriented YSZ substrates, respectively.[1] Scale bars are 1 μm. (c,d) The corresponding length for NWs in (a,b) as a function of catalyst diameter. (e,f) The square root of growth velocity of NWs in (a,b) as a function of reciprocal of catalyst diameter. The cutoff diameters are denoted in (c,d).

Effects of Growth Conditions on the Cutoff Parameters:

We should note here that the cutoff diameters in this work are larger than those reported in our previous paper,[1] which is a result of the different growth conditions. Here, the ITO NWs grow at a growth pressure of 30 mbar and a growth temperature of 850 ºC; in contrast, in our previous paper, the ITO NWs grow during the cooling down process from 900 ºC to 800 ºC at a growth pressure of 1 mbar. According to the equation for cutoff diameter, $d_c = 4\Omega\alpha_{vs}/\Delta\mu_0$, the value is determined by two factors, the surface energy and the supersaturation between vapor and solid with infinite radius of curvature, for a given NW growth system. In general, higher growth temperature leads to higher vapor pressure and chemical potential, and thus smaller cut-off diameter if we assume the influence of the growth temperature on the surface and interface energies is not as significant. In fact, smaller cut-off diameter could be achieved if we increased further both growth temperature and pressure because higher growth pressure should lead to lower surface energy and smaller cutoff diameter. In our future works, we will explore in detail the complex influences of the growth parameters, i.e., temperature, pressure and doping, on the growth thermodynamics.

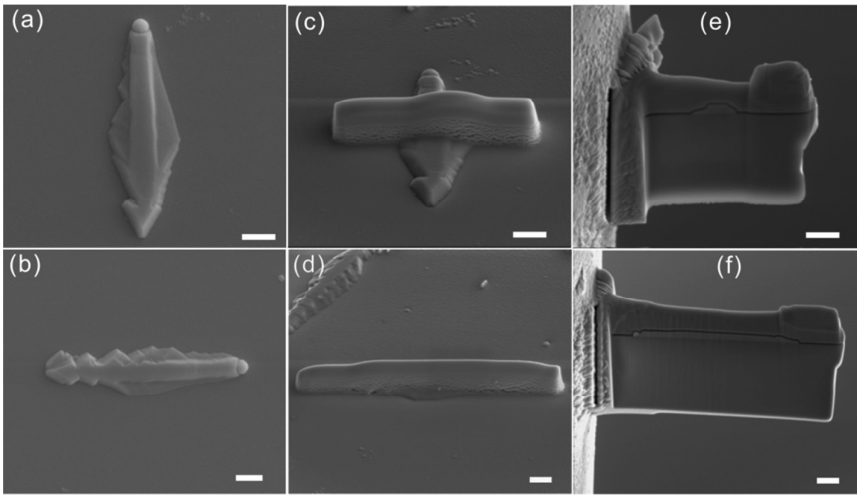

Figure S4. SEM images showing the preparation procedure for axial and lateral cross-sectional TEM analysis by using focused ion beam (FIB) milling and in-situ lift-out (INLO). (a,b) SEM image of ITO nanostructure prior to FIB milling. (c,d) 400 nm SiO_2 and 50 nm Pt were deposited atop the samples to prevent damage of interested area under ion beams. (e,f) The FIB cut lamella was transferred from home substrate to the copper TEM grid. During the FIB, a 30keV Ga beam was used for rough milling and reduced voltage (5keV) was used for fine milling. Samples were further cleaned with low angle Ar ion milling. Scale bars: 1 μm in (a-f).

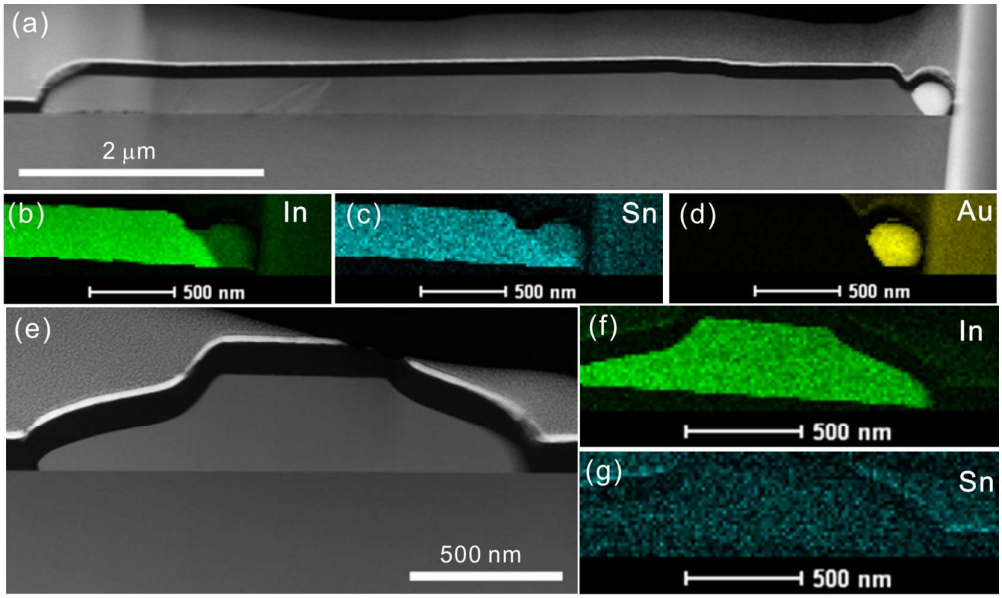

Figure S5. **The elemental analysis of axial and lateral cross-section.** (a) The morphology of lateral cross-section. (b-d) EDX elemental (In, Sn and Au) mapping of lateral cross-section. (e) The morphology of axial cross-section. (f,g) EDX elemental (In and Sn) mapping of axial cross-section. The EDX mappings show that tin dopants are distributed uniformly.

Derivation of the Modified Gibbs-Thomson Equations:

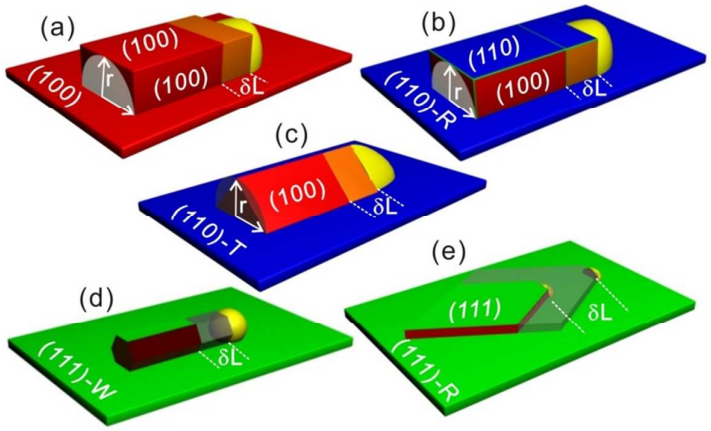

Schematics illustrating the growth mechanism of ITO NWs

◆ **Model (a) for rectangular planar NWs grown on a (100) substrate:**

The volume of NW can be written as:

$$\mathrm{V} = \mathrm{r} \times 2\mathrm{r} \times \mathrm{L} = 2r^2 L$$

When the length L increases to L+ΔL, the volume change can be written as:

$$\Delta\mathrm{V} = 2r^2 \Delta L$$

So the change in the number of atoms is written as:

$$\Delta\mathrm{N} = \frac{\Delta V}{\Omega} = \frac{2r^2 \Delta L}{\Omega} \qquad \text{(a1)}$$

The Gibbs free energy changes during NWs growth can be expressed as:

$$\Delta\mathrm{G} = \Delta\mathrm{N}\,(-\Delta\mu_0) + \Delta S_{vs}\alpha_{vs} + \Delta S_{inter}\alpha_{inter} - \Delta S_{inter}\alpha_{ysz} \qquad \text{(a2)}$$

The supersaturation is given as:

$$\Delta\mu = -\frac{\Delta G}{\Delta N} = \Delta\mu_0 - \frac{\Delta S_{vs}\alpha_{vs} + \Delta S_{inter}\alpha_{inter} - \Delta S_{inter}\alpha_{ysz}}{\Delta\mathrm{N}} \qquad \text{(a3)}$$

We can also write:

$$\Delta S_{vs}\alpha_{vs} = 4r\Delta L \times \alpha_{vs,(100)}$$

$$\Delta S_{inter}\alpha_{inter} = 2r\Delta L \times \alpha_{inter,(100)}$$

$$\Delta S_{inter}\alpha_{ysz} = 2r\Delta L \times \alpha_{ysz,(100)}$$

Once these equations are substituted into (a3), the supersaturation can be re-written as:

$$\Delta\mu = \Delta\mu_0 - \frac{\Omega}{d}(4\alpha_{vs,(100)} + 2\alpha_{inter,(100)} - 2\alpha_{ysz,(100)}) \quad \text{(a4)}$$

- **Model (b), for [110]-oriented NWs with rectangular cross-section grown on a (110) substrate:**

The volume of NW can be written as:

$$\mathrm{V} = \mathrm{r} \times 2\mathrm{r} \times \mathrm{L} = 2r^2L$$

When the length L increases to L+ΔL, the volume change can be written as:

$$\Delta\mathrm{V} = 2r^2\Delta L$$

So the change in the number of atoms is written as:

$$\Delta\mathrm{N} = \frac{\Delta V}{\Omega} = \frac{2r^2\Delta L}{\Omega} \quad \text{(b1)}$$

The Gibbs free energy changes during NWs growth can be expressed as:

$$\Delta\mathrm{G} = \Delta\mathrm{N}\,(-\Delta\mu_0) + \Delta S_{vs}\alpha_{vs} + \Delta S_{inter}\alpha_{inter} - \Delta S_{inter}\alpha_{ysz} \quad \text{(b2)}$$

The supersaturation is given as:

$$\Delta\mu = -\frac{\Delta G}{\Delta N} = \Delta\mu_0 - \frac{\Delta S_{vs}\alpha_{vs} + \Delta S_{inter}\alpha_{inter} - \Delta S_{inter}\alpha_{ysz}}{\Delta\mathrm{N}} \quad \text{(b3)}$$

We can also write:

$$\Delta S_{vs}\alpha_{vs} = 2r\Delta L \times \alpha_{vs,(110)} + 2r\Delta L \times \alpha_{vs,(100)}$$

$$\Delta S_{inter}\alpha_{inter} = 2r\Delta L \times \alpha_{inter,(110)}$$

$$\Delta S_{inter}\alpha_{ysz} = 2r\Delta L \times \alpha_{ysz,(110)}$$

Once these equations are substituted into (b3), the supersaturation can be re-written as:

$$\Delta\mu = \Delta\mu_0 - \frac{\Omega}{d}(2\alpha_{vs,(100)} + 2\alpha_{vs,(110)} + 2\alpha_{inter,(110)} - 2\alpha_{ysz,(110)}) \quad \text{(b4)}$$

- **Model (c), for [100]-oriented NWs with triangle cross-section grown on a (110) substrate:**

The volume of NW can be written as:

$$\mathrm{V} = \frac{1}{2} \times \mathrm{r} \times 2\mathrm{r} \times \mathrm{L} = r^2L$$

When the length L increases to L+ΔL, the volume change can be written as:

$$\Delta V = r^2 \Delta L$$

So the change in the number of atoms is written as:

$$\Delta N = \frac{\Delta V}{\Omega} = \frac{r^2 \Delta L}{\Omega} \quad \text{(c1)}$$

The Gibbs free energy changes during NWs growth can be expressed as:

$$\Delta G = \Delta N\,(-\Delta\mu_0) + \Delta S_{vs}\alpha_{vs} + \Delta S_{inter}\alpha_{inter} - \Delta S_{inter}\alpha_{ysz} \quad \text{(c2)}$$

The supersaturation is given as:

$$\Delta\mu = -\frac{\Delta G}{\Delta N} = \Delta\mu_0 - \frac{\Delta S_{vs}\alpha_{vs} + \Delta S_{inter}\alpha_{inter} - \Delta S_{inter}\alpha_{ysz}}{\Delta N} \quad \text{(c3)}$$

We can also write:

$$\Delta S_{vs}\alpha_{vs} = 2 \times \sqrt{2} r \Delta L \times \alpha_{vs,(100)}$$

$$\Delta S_{inter}\alpha_{inter} = 2 r \Delta L \times \alpha_{inter,(110)}$$

$$\Delta S_{inter}\alpha_{ysz} = 2 r \Delta L \times \alpha_{ysz,(110)}$$

Once these equations are substituted into (c3), the supersaturation can be re-written as:

$$\Delta\mu = \Delta\mu_0 - \frac{\Omega}{d}\left(4\sqrt{2}\alpha_{vs,(100)} + 4\alpha_{inter,(110)} - 4\alpha_{ysz,(110)}\right) \quad \text{(c4)}$$

◆ **Model (d), for wire-shaped nanostructure grown on a (111) substrate:**

As shown in the following figure, the cross-section of (111)-W NW is hexagonal with sidewall of {113} planes. This is deduced from the fact that the angle formed between (111) and (1-13) planes is 121.5º, very close to 120º. In order to simply the calculation, we assume the angle between the top plane and side wall is 120º and the hexagonal is a regular hexagonal.

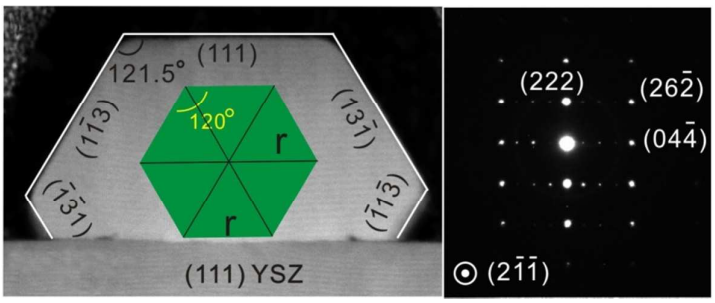

So the volume of NW can be written as:

$$\mathrm{V} = 6 \times (\frac{1}{2} \times \mathrm{r} \times \frac{\sqrt{3}}{2}\mathrm{r}) \times \mathrm{L} = \frac{3\sqrt{3}}{2} r^2 L$$

When the length L increases to L+ΔL, the volume change can be written as:

$$\Delta\mathrm{V} = \frac{3\sqrt{3}}{2} r^2 \Delta L$$

So the change in the number of atoms is written as:

$$\Delta\mathrm{N} = \frac{\Delta V}{\Omega} = \frac{\frac{3\sqrt{3}}{2} r^2 \Delta L}{\Omega} \quad \text{(d1)}$$

The Gibbs free energy changes during NWs growth can be expressed as:

$$\Delta\mathrm{G} = \Delta\mathrm{N}\,(-\Delta\mu_0) + \Delta S_{vs}\alpha_{vs} + \Delta S_{inter}\alpha_{inter} - \Delta S_{inter}\alpha_{ysz} \quad \text{(d2)}$$

The supersaturation is given as:

$$\Delta\mu = -\frac{\Delta G}{\Delta N} = \Delta\mu_0 - \frac{\Delta S_{vs}\alpha_{vs} + \Delta S_{inter}\alpha_{inter} - \Delta S_{inter}\alpha_{ysz}}{\Delta\mathrm{N}} \quad \text{(d3)}$$

We can also write:

$$\Delta S_{vs}\alpha_{vs} = 4 \times r\Delta L \times \alpha_{vs,(113)} + r\Delta L \times \alpha_{vs,(111)}$$

$$\Delta S_{inter}\alpha_{inter} = r\Delta L \times \alpha_{inter,(111)}$$

$$\Delta S_{inter}\alpha_{ysz} = r\Delta L \times \alpha_{ysz,(111)}$$

Once these equations are substituted into (d3), the supersaturation can be re-written as:

$$\Delta\mu = \Delta\mu_0 - \frac{\Omega}{d}(\frac{16}{3\sqrt{3}}\alpha_{vs,(113)} + \frac{4}{3\sqrt{3}}\alpha_{vs,(111)} + \frac{4}{3\sqrt{3}}\alpha_{inter,(111)} - \frac{4}{3\sqrt{3}}\alpha_{ysz,(111)}) \quad \text{(d4)}$$

◆ **Model (e), for rhombus-shaped nanostructure grown on a (111) substrate:**

When the length of (111)-R is L, the width is $L/\sqrt{3}$ according to the rhombus geometry relationship. The surface area and volume of NW can be written as:

$$\mathrm{S} = \mathrm{L} \times \frac{L}{2\sqrt{3}} + 4 \times \frac{L}{\sqrt{3}} \times (2\mathrm{r}) = \frac{1}{2\sqrt{3}} L^2 + \frac{2}{\sqrt{3}} Lr$$

$$\mathrm{V} = \mathrm{r} \times \mathrm{L} \times \frac{L}{2\sqrt{3}} = \frac{1}{2\sqrt{3}} rL^2$$

When the length L increases to L+ΔL, the surface area and volume changes can be written as:

$$\Delta S = \frac{1}{\sqrt{3}} L\Delta L + \frac{2}{\sqrt{3}} r\Delta L \approx \frac{1}{\sqrt{3}} L\Delta L \qquad \text{(because L} \gg \text{r)}$$

$$\Delta V = \frac{1}{\sqrt{3}} rL\Delta L$$

So the change in the number of atoms is written as:

$$\Delta N = \frac{\Delta V}{\Omega} = \frac{\frac{1}{\sqrt{3}} rL\Delta L}{\Omega} \tag{e1}$$

The Gibbs free energy changes during NWs growth can be expressed as:

$$\Delta G = \Delta N\,(-\Delta\mu_0) + \Delta S_{vs}\alpha_{vs} + \Delta S_{inter}\alpha_{inter} - \Delta S_{inter}\alpha_{ysz} \tag{e2}$$

The supersaturation is given as:

$$\Delta\mu = -\frac{\Delta G}{\Delta N} = \Delta\mu_0 - \frac{\Delta S_{vs}\alpha_{vs} + \Delta S_{inter}\alpha_{inter} - \Delta S_{inter}\alpha_{ysz}}{\Delta N} \tag{e3}$$

We can also write:

$$\Delta S_{vs}\alpha_{vs} = \frac{1}{\sqrt{3}} L\Delta L \times \alpha_{vs,(111)}$$

$$\Delta S_{inter}\alpha_{inter} = \frac{1}{\sqrt{3}} L\Delta L \times \alpha_{inter,(111)}$$

$$\Delta S_{inter}\alpha_{ysz} = \frac{1}{\sqrt{3}} L\Delta L \times \alpha_{ysz,(111)}$$

Once these equations are substituted into (e3), the supersaturation can be re-written as:

$$\Delta\mu = \Delta\mu_0 - \frac{\Omega}{d}\left(2\alpha_{vs,(111)} + 2\alpha_{inter,(111)} - 2\alpha_{ysz,(111)}\right) \tag{e4}$$

Reference:

(1) Shen, Y. D.; Turner, S.; Yang, P.; Van Tendeloo, G.; Lebedev, O. I.; Wu, T. Nano Lett. 2014, 14 (8), 4342-4351.